Assessment of vibro-acoustic sound emissions based on structural dynamics

Andreas Wurzinger[1], Florian Kraxberger[1], Bernhard Mayr-Mittermüller[2], Péter Rucz[3], Harald Sima[2], Manfred Kaltenbacher[1], Stefan Schoder[1]

[1] *Graz University of Technology, IGTE, A-8010 Graz, Austria, Email: andreas.wurzinger@tugraz.at*

[2] *Otto Bock Healthcare Products GmbH, A-1110 Wien, Austria*

[3] *Budapest University of Technology and Economics, HIT, H-1111 Budapest, Hungary*

Introduction

Quantification of sound generation of complex mechanical devices is of major significance during the design process in order to improve customer comfort or meet legal requirements. For any device with direct user interaction, noise emissions can have multiple negative effects on the user and the user's environment [1]. Therefore, tools to predict and quantify sound emissions should be integrated in an early design stage. For many applications, direct measurement of the radiated sound field using microphone arrays is not feasible. However, surface vibrations of the mechanical structure can often be computed by the finite element method or measured by the use of Laser-Doppler Scanning Vibrometry (LSV), respectively. Subsequently, the Boundary Element Method (BEM) can be used to simulate sound propagation based on the surface vibration velocity.

In the scope of this contribution, a workflow to predict the radiated sound field using arbitrary information about the structural dynamics is presented. A more in-depth description and validation of the presented workflow was given in [2]. The workflow is depicted in Fig. 1. In the first step, the acquired information about the structural vibration is transformed onto a closed surface modeling the radiation domain boundary. Secondly, the exterior sound propagation problem is solved using the BEM. Finally, post-processing of the simulation result allows to quantify and easily compare different designs. In the following, the workflow is presented, applied, and validated on a complex housing part of a mechatronic knee prosthesis.

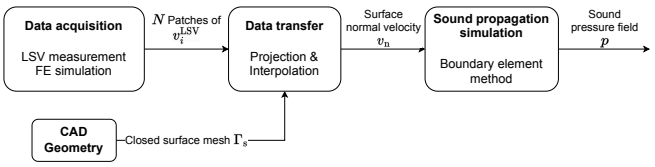

Figure 1: Workflow of the sound radiation simulation based on the structural dynamics of the vibrating body [2, Fig. 1].

Data acquisition and transfer

The surface normal velocity, required as a boundary condition for the acoustic propagation model, can be obtained efficiently by LSV measurements, as depicted schematically in Fig. 2. Thereby, the surface velocity in the laser direction $v_j^{\mathrm{LSV}} = \boldsymbol{v} \cdot \boldsymbol{n}_j^{\mathrm{LSV}}$ can be measured, where $\boldsymbol{n}_j^{\mathrm{LSV}}$ denotes the unit vector in the laser direction, and j the index of the measured surface location. When dealing with nearly flat surfaces, it can be sufficient to position the laser scanning head in the dominant direction of overall normal motion and use this velocity component to approximate the normal velocity v_{n}. Different scanning

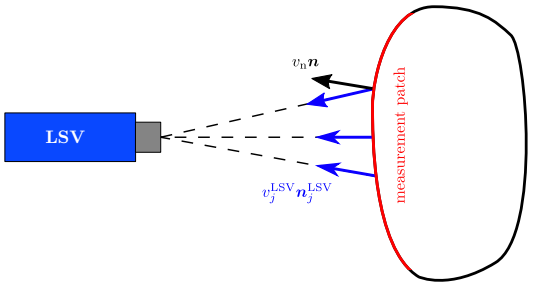

Figure 2: Sketch of an experimental setup using a laser scanning vibrometer (LSV) [2, Fig. 2].

head positions result in N patches of measurement data. Regarding the sound propagation simulation, the measured data must be transferred to a closed (and most often refined) surface representation. Challenges for this data transfer include (i) imperfect representation of the geometry by the measured surface patch, (ii) spatial upsampling of coarsely distributed measurement data, and (iii) overlapping data patches.

In [2], a two-step data transfer process is proposed, consisting of a projection and an interpolation step, which is combined into a linear transformation $\boldsymbol{T}_i$ for each measurement patch i. In the following, the mesh of the closed geometry used for simulation is denoted by *target* Γ^{t}, and patch i containing measurement data is denoted by *source* Γ_i^{s}. The algorithm to obtain the transformation matrix $\boldsymbol{T}_i$ is described in [2, Alg. 1], and is depicted in Fig. 3. It can be summarized as follows: For any given point

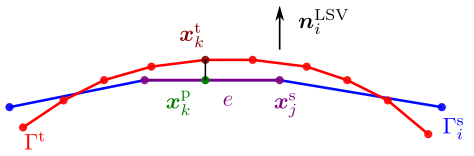

Figure 3: Sketch of an arbitrary source (blue) and target mesh (red) with indicated point projection from the target to the source mesh [2, Fig. 3].

$\boldsymbol{x}_k^{\mathrm{t}}$ on the target mesh, the location is projected in the measurement direction onto the source mesh. For simplicity, the measurement direction used for the projection is averaged over all points in a patch, resulting in a mean direction $\boldsymbol{n}_i^{\mathrm{LSV}}$. Next, linear shape functions $N_j(\boldsymbol{x})$ (e.g., see [3]) are evaluated for the projected point $\boldsymbol{x}_k^{\mathrm{p}}$ in the

according element e. In this context, the (linear) shape function evaluation can also be used to check whether the projected point is inside any element. Finally, the shape function values are used as transformation coefficients corresponding to the source grid point indices and the index of the target point

$$\boldsymbol{T}_i = [T_{j,k}] = [N_j(\boldsymbol{x}_k^{\mathrm{p}})] \quad \forall j \in e \in \Gamma^{\mathrm{s}} \wedge \forall k \in \Gamma^{\mathrm{t}}\,. \tag{1}$$

In the scope of this work, the acoustic radiation of a clinically applied knee prosthesis frame is investigated by means of measurements and simulations. The prosthesis frame (device under test — DUT) has dimensions ($0.27 \times 0.08 \times 0.1\,\mathrm{m}$) and is made of carbon-fiber-reinforced plastic with titanium inserts. The complex material behavior complicates an accurate prediction of the structural dynamics using FE simulation, and experimental acquisition of the surface vibration is preferred. A detailed description of the conducted measurements is given in [2] and shall be summarized in the following.

The DUT is positioned on a table with the shaker (*DynaLabs DYN-PM-100*), which is connected to the DUT by a stinger. The shaker is mounted on rubber elements to decouple it mechanically from the table. To measure the input force, an impedance head (*DJB AF/100/10*) is applied at the stinger-DUT connection, allowing for measurements of the excitation force F on the DUT. The surface velocity of the DUT is measured using an LSV (*Polytec PSV-500 Xtra*) from four positions, as indicated in Fig. 4. This results in an overall number of measurement points $N_{\mathrm{LSV}} = 688$, at which the H1 approximate of the mobility transfer function $Y^v_{\mathrm{H1}} \approx \frac{v}{F}$ is evaluated in the frequency range $f = [2, 6400]\,\mathrm{Hz}$.

Sound radiation

To model the sound emissions of the vibrating body under investigation, a simulation setup was established using the open-source BEM library NiHu [4]. Therewith, the Helmholtz boundary integral equation

$$Cp_{\mathrm{a}} = \int_{\Gamma_{\mathrm{s}}} \left(p_{\mathrm{a}} \frac{\partial G}{\partial y_i} - G \frac{\partial p_{\mathrm{a}}}{\partial y_i} \right) \cdot \boldsymbol{n}\, \mathrm{d}\Gamma \tag{2}$$

is solved with the fluctuating acoustic pressure p_{a}, the Green's function $G(\boldsymbol{x}|\boldsymbol{y}, k)$ for 3D acoustic radiation

$$G(\boldsymbol{x}|\boldsymbol{y}, k) = \frac{1}{4\pi|\boldsymbol{x}-\boldsymbol{y}|} e^{-\mathrm{j}k|\boldsymbol{x}-\boldsymbol{y}|}\,, \tag{3}$$

with $\boldsymbol{x}$ and $\boldsymbol{y}$ being the receiver and source points respectively and $k = \frac{\omega}{c_0}$ is the wave number, with an isentropic speed of sound $c_0 = 343\,\frac{\mathrm{m}}{\mathrm{s}}$, and $C = 0.5$ to represent the boundary as a smooth surface [5]. The vibrating surface was modeled with a Neumann boundary condition

$$\Gamma_{\mathrm{s}} \;:\; \frac{\partial p_{\mathrm{a}}}{\partial n_i} = \rho_0\, j\omega\, \boldsymbol{v}_{\mathrm{s}} \cdot \boldsymbol{n}\,, \tag{4}$$

with angular frequency ω, mean density of air at ambient conditions $\rho_0 = 1.225\,\frac{\mathrm{kg}}{\mathrm{m}^3}$ and the surface velocity $\boldsymbol{v}_{\mathrm{s}}$. The mobility transfer function was used to compute the vibroacoustic transfer function $Y^p_{\mathrm{H1}} \approx \frac{p_{\mathrm{a}}}{F}$, representing the acoustic pressure field based on a unit force excitation. As

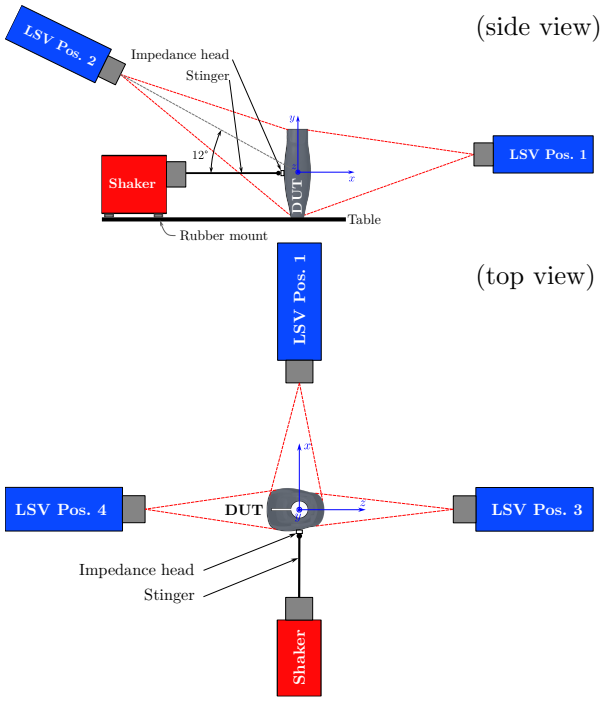

Figure 4: Sketch of the experimental setup with the LSV. The coordinate system's origin is located in the center of the device under test (DUT), such that the excitation force vector lies inside the x/z plane. The LSV is positioned approximately 0.7 m from the DUT [2, Fig. 9].

with the conventional BEM spurious modes occur towards high frequencies, the Burton-Miller method [6] was used to solve the problem. The discretized equations are given in [2].

For reference, additional microphone measurements were conducted corresponding to the sketch in Fig. 5. A detailed description of the reference measurements and discussion thereof can be found in [2], and are briefly summarized in the following. The measurement environment is an acoustically treated chamber of type *Studiobox Premium* with size ($3.0 \times 2.02 \times 2.3\,\mathrm{m}$). The prosthesis frame (DUT) is positioned centrally in the room on a table which is acoustically treated at the top and bottom surface to attenuate room modes and ensure field field conditions. Furthermore, an acoustically treated box is put over the shaker to minimize the influence of the sound emissions of the shaker on the measurement setup. In the following, only microphone 1 (*Brüel & Kjaer 4189 free-field microphone*), placed at a distance of $l_{\mathrm{mic}} = 0.7\,\mathrm{m}$ from the DUT is considered. Comprehensive validation of the using the measurement data was done in [2]. The measured pressure time series was transformed into the frequency domain, and the H1 estimate of the vibroacoustic transfer function $Y^p_{\mathrm{H1}} \approx \frac{p_{\mathrm{a}}}{F}$ is computed.

Figure 6 depicts the H1 estimate of the vibroacoustic transfer function based on microphone measurement (in grey) and based on the presented workflow using measured surface velocities and sound propagation simulation (in orange). In general, good agreement between the two workflows is achieved in the frequency range $f = [500, 5000]\,\mathrm{Hz}$. Resonance peaks in the transfer func-

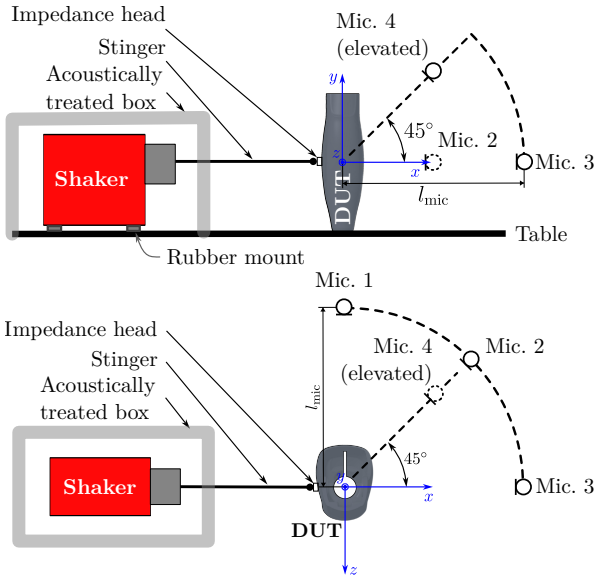

Figure 5: Sketch of the experimental setup for the microphone measurements. Mic. 1, 2, and 3 are located in the x/z plane. Mic. 4 is at 45° elevation above mic. 2. The coordinate system's origin is located in the center of the DUT.[2, Fig. 8]

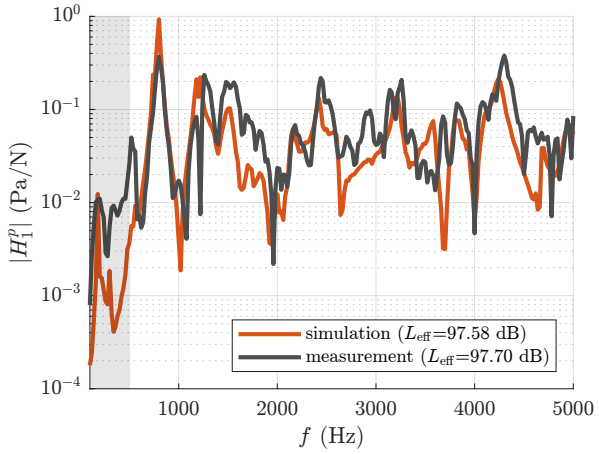

Figure 6: H_1^{p} transfer functions based on microphone measurements and LSV measurements in combination with the BEM simulation, according to [2, Fig. 11a] The effective pressure level (according to [2, Eq. (11)]) was evaluated for $f = [500, 5000]$ Hz.

tion due to resonance of the structural-mechanical system, the acoustic system, or coupled resonance are captured equally well, especially at medium frequencies. In the low-frequency range below 500 Hz, the microphone measurement overestimates the transfer function compared to the simulation approach. This behavior is probably caused by the inefficient decoupling of the shaker from the measurement environment both mechanically via induced vibrations to the table and acoustically due to insufficient acoustic insulation of the shaker [2].

Radiated sound power

The radiated sound power is computed as an integral metric to assess the radiation property of the DUT to the acoustic far field. It can be computed directly from the solved boundary problem with Eq. (5) by the use of $v_{\mathrm{n}} = \frac{\partial p_{\mathrm{a}}}{\partial \boldsymbol{n}}$. Alternatively, there are other computationally less expensive approximation methods, e.g., see [7]. In this investigation, the radiated sound power estimates based on the *Equivalent Radiated Power* (ERP), see Eq. (6), and based on the *Volume Velocity* (VV), see Eq. (7), are considered.

$$P_{\mathrm{BEM}} = \frac{1}{2}\int_{\Gamma_{\mathrm{s}}} \Re\left\{p_{\mathrm{a}} v_{\mathrm{n}}^*\right\} \mathrm{d}\Gamma \tag{5}$$

$$P_{\mathrm{ERP}} = \frac{1}{2}\rho c_0 \int_{\Gamma_{\mathrm{s}}} |v_{\mathrm{n}}|^2 \mathrm{d}\Gamma \tag{6}$$

$$P_{\mathrm{VV}} = \frac{k^2 \rho c_0}{4\pi}\left[\int_{\Gamma_{\mathrm{s}}} v_{\mathrm{n}} \mathrm{d}\Gamma\right]^2 \tag{7}$$

Furthermore, the ratio of radiated to total sound power is given by the radiation efficiency

$$\eta = \frac{\int_{\Gamma_{\mathrm{s}}} \Re\left\{p_{\mathrm{a}} v_{\mathrm{n}}^*\right\} \mathrm{d}\Gamma}{\int_{\Gamma_{\mathrm{s}}} \left|p_{\mathrm{a}} v_{\mathrm{n}}^*\right| \mathrm{d}\Gamma}\,. \tag{8}$$

The two low-cost approximations can be understood as qualitative upper and lower bounds for vibroacoustically emitted sound power. The ERP uses the far-field approximation, resulting in a constant radiation efficiency $\eta = 1$ of all surface areas and neglects local acoustic effects that can occur in the near-field. Therefore, dipole effects (antiphase vibration of the sources) are not captured, and the radiated sound power is overestimated in the low-frequency range. Towards higher frequencies, these effects are less significant, and thus the deviation decreases. In contrast, the VV assumes an acoustically compact source, which is only viable in the very low-frequency range. Both estimates can be evaluated explicitly as simple summations without the need to assemble a system matrix and thus can be computed in the order of seconds on any state-of-the-art notebook [2]. In Fig. 7, the two estimates and the BEM solution are depicted together with the radiation efficiency.

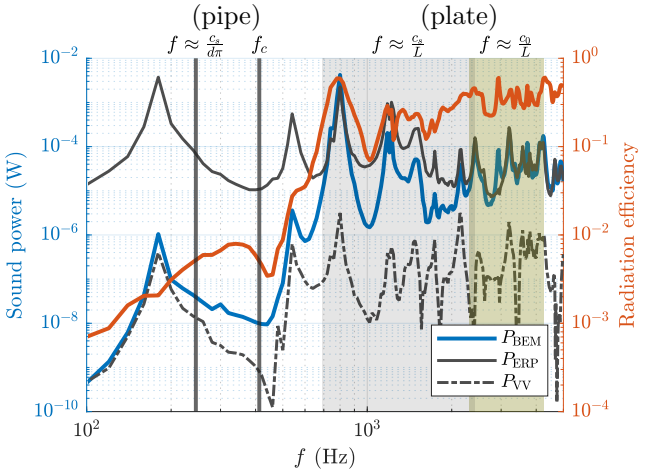

Figure 7: Radiated sound power of the DUT (left axis) computed from BEM simulation (blue) in comparison with low-cost approximations (grey). The right axis shows the radiation efficiency (orange).

To investigate potential frequency limits of the low-cost sound power estimates ERP and VV, a simple oscillating thin square steel plate with dimensions ($1 \times 1 \times 0.01$ m),

that is supported on one edge and excited by a point force at an arbitrary position is considered. The material is defined by density $\rho = 7872\,\frac{\mathrm{kg}}{\mathrm{m}^3}$, Young's modulus $E = 2 \times 10^{11}\,\mathrm{Pa}$, and Poisson number $\nu = 0.29$. Figure 8 depicts the radiated sound power and the radiation efficiency over the Helmholtz number $\mathrm{He} = \frac{L}{\lambda} = \frac{fL}{c_0}$, respectively. Again, ERP and VV can be interpreted as low

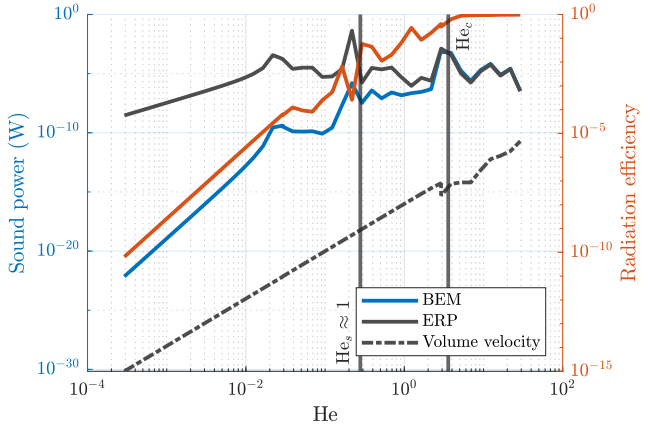

Figure 8: Radiated sound power of an oscillating plate (left axis) computed from BEM simulation in comparison with approximations equivalent radiated power P_{ERP}, and volume velocity based sound power P_{VV}. The right axis shows the radiation efficiency (orange).

and high-frequency limits of the radiated sound power, although it is noted that the radiation is dominated by pure flexural vibration, and therefore, the VV predicts negligible sound power (which is the correct limit for $f \to 0$, however, this is a trivial finding). On the other hand, at He numbers above 1, the radiation efficiency approaches 1, which gives a potential limit of the ERP. If the phase speed of the structural wave is considered based on the Kirchhoff-Love shell theory,

$$c_s = \sqrt[4]{\frac{S_x \omega^2}{A_x \rho \left(1 - \nu^2\right)}}\,, \tag{9}$$

with flexural stiffness S_x and cross-section area A_x, an alternative Helmholtz number $\mathrm{He}_s = \frac{fL}{c_s}$ can be defined which indicates a slightly lower frequency. Furthermore, the well-known coincidence frequency, which is defined by the matching phase speed of the acoustic and flexural wave, gives a good estimate.

To apply these findings on the DUT, the geometry was approximated by (i) a plate of dimensions $(0.15 \times 0.05 \times 0.005\,\mathrm{m})$, or (ii) a pipe of diameter $d = 0.08\,\mathrm{m}$, wall thickness $t = 0.005\,\mathrm{m}$, and length $L = 0.25\,\mathrm{m}$. For the plate approximation, the coincidence frequency computes as $f_c \approx 7.6\,\mathrm{kHz}$, while the frequency ranges $\mathrm{He} \approx 1$, and $\mathrm{He}_s \approx 1$ are indicated as shaded areas in Fig. 7. For the pipe approximation, the ring area was used to compute the flexural phase speed, which results in a significant underestimation of the validity limit of the ERP estimate, as depicted in Fig. 7.

Conclusion

In this work, a workflow to predict sound emissions of a device is presented, using arbitrary information about the body vibration as prior knowledge. The workflow consisting of the two-stage data transformation and subsequent sound propagation simulation using the BEM was applied to an industrial problem and validated at certain locations via reference microphone measurements. Furthermore, the sound field was used to compute the radiated sound power. The BEM-based sound power prediction is compared to common low-cost estimates, and possible frequency limits of these estimates are discussed based on a simple oscillating plate problem and the application example.

Acknowledgment

This project has received funding from the Austrian Research Promotion Agency (FFG) under the Bridge project No. [71694].

Bibliography

[1] S. Kumar, H. M. Forster, P. Bailey, and T. D. Griffiths. Mapping unpleasantness of sounds to their auditory representation. *The Journal of the Acoustical Society of America*, 124(6):3810–3817, December 2008. ISSN: 0001-4966. DOI: 10.1121/1.3006380.

[2] A. Wurzinger, F. Kraxberger, P. Maurerlehner, B. Mayr-Mittermüller, P. Rucz, H. Sima, M. Kaltenbacher, and S. Schoder. Experimental Prediction Method of Free-Field Sound Emissions Using the Boundary Element Method and Laser Scanning Vibrometry. *Acoustics*, 6(1):65–82, March 2024. ISSN: 2624-599X. DOI: 10.3390/acoustics6010004.

[3] M. Kaltenbacher. *Numerical Simulation of Mechatronic Sensors and Actuators: Finite Elements for Computational Multiphysics*. Springer Berlin Heidelberg, Berlin, Heidelberg, 3rd edition, 2015. ISBN: 978-3-642-40170-1. DOI: 10.1007/978-3-642-40170-1.

[4] P. Fiala and P. Rucz. NiHu: An open source C++ BEM library. *Advances in Engineering Software*, 75:101–112, September 2014. ISSN: 09659978. DOI: 10.1016/j.advengsoft.2014.05.011.

[5] S. Marburg. Boundary Element Method for Time-Harmonic Acoustic Problems. In M. Kaltenbacher, editor, *Computational Acoustics*, CISM International Centre for Mechanical Sciences, pages 69–158. Springer International Publishing, Cham, 2018. ISBN: 978-3-319-59038-7. DOI: 10.1007/978-3-319-59038-7_3.

[6] A. J. Burton and G. F. Miller. The application of integral equation methods to the numerical solution of some exterior boundary-value problems. *Proceedings of the Royal Society of London*, 323:201–210, 1971. DOI: 10/b36r2q.

[7] D. Fritze, S. Marburg, and H.-J. Hardtke. Estimation of Radiated Sound Power: A Case Study on Common Approximation Methods. *Acta Acustica united with Acustica*, 95(5):833–842, September 2009. DOI: 10.3813/AAA.918214.